

Brief Report

Binding Parameters of [¹¹C]MPC-6827, a Microtubule-Imaging PET Radiopharmaceutical in Rodents

Avinash H. Bansode ^{1,†} , Bhuvanachandra Bhoopal ^{1,†}, Krishna Kumar Gollapelli ¹, Naresh Damuka ¹, Ivan Krizan ¹, Mack Miller ¹, Suzanne Craft ², Akiva Mintz ³ and Kiran Kumar Solingapuram Sai ^{1,*} ¹ Department of Radiology, Wake Forest School of Medicine, Winston Salem, NC 27157, USA² Department of Gerontology, Wake Forest School of Medicine, Winston Salem, NC 27157, USA³ Department of Radiology, Columbia Medical Center, New York, NY 10032, USA

* Correspondence: ksolinga@wakehealth.edu; Tel.: +1-3367165630

† These authors contributed equally to this work.

Abstract: Impairment and/or destabilization of neuronal microtubules (MTs) resulting from hyperphosphorylation of the tau proteins is implicated in many pathologies, including Alzheimer's disease (AD), Parkinson's disease and other neurological disorders. Increasing scientific evidence indicates that MT-stabilizing agents protect against the deleterious effects of neurodegeneration in treating AD. To quantify these protective benefits, we developed the first brain-penetrant PET radiopharmaceutical, [¹¹C]MPC-6827, for *in vivo* quantification of MTs in rodent and nonhuman primate models of AD. Mechanistic insights revealed from recently reported studies confirm the radiopharmaceutical's high selectivity for destabilized MTs. To further translate it to clinical settings, its metabolic stability and pharmacokinetic parameters must be determined. Here, we report *in vivo* plasma and brain metabolism studies establishing the radiopharmaceutical-binding constants of [¹¹C]MPC-6827. Binding constants were extrapolated from autoradiography experiments; pretreatment with a non-radioactive MPC-6827 decreased the brain uptake >70%. It exhibited ideal binding characteristics (typical of a CNS radiopharmaceutical) including LogP (2.9), K_d (15.59 nM), and B_{max} (11.86 fmol/mg). Most important, [¹¹C]MPC-6827 showed high serum and metabolic stability (>95%) in rat plasma and brain samples.



Citation: Bansode, A.H.; Bhoopal, B.; Gollapelli, K.K.; Damuka, N.; Krizan, I.; Miller, M.; Craft, S.; Mintz, A.; Solingapuram Sai, K.K. Binding Parameters of [¹¹C]MPC-6827, a Microtubule-Imaging PET Radiopharmaceutical in Rodents. *Pharmaceuticals* **2023**, *16*, 495.

<https://doi.org/10.3390/ph16040495>

Academic Editor: Martina Benešová

Received: 24 February 2023

Revised: 18 March 2023

Accepted: 21 March 2023

Published: 27 March 2023



Copyright: © 2023 by the authors. Licensee MDPI, Basel, Switzerland. This article is an open access article distributed under the terms and conditions of the Creative Commons Attribution (CC BY) license (<https://creativecommons.org/licenses/by/4.0/>).

Keywords: PET imaging; microtubules; radiochemistry; metabolism; stability; translational molecular imaging

1. Introduction

Alzheimer's disease (AD) is recognized by the formation of extracellular amyloid plaques and intracellular hyperphosphorylated tau, a microtubule-associated protein (MAP) [1,2]. Changes in tau protein in axonal region (axonal MAP) are associated with AD and other related dementia disorders [3–13]. Tau normally functions as a bridge, ensuring that MTs in axons run straight and parallel to one another. In the pathological changes implicated in AD and related dementias, tau detaches from MTs and accumulates in the neuronal cell body [14,15]. The flow of information in the neurons is affected due to withering of axons caused by the disruption of cytoskeleton [16]. Additionally, MT dynamics contribute to changes in neuronal polarities, altering MAP distribution and resulting in neurodegeneration events [17]. MT stability is disrupted early in AD and other related dementias, primarily when abnormal A β and tau modifications sequester MAPs. Taken together, these findings suggest that MT dysfunction connects A β /tau-based degenerative events to the hallmark pathologies of AD. Therefore, quantifying MT dynamics is critical in understanding early neurodegenerative cascade of AD [17,18].

Neuroimaging has revolutionized the identification and quantification of molecular changes during neurodegeneration and currently available A β and tau PET can characterize disease lesions [19–21]. We hypothesized that MT-based PET can target early

molecular events contributing to AD pathophysiology, which is considered a key gap in the understanding of MT structural changes inherent to AD pathophysiology.

MPC-6827 is a high-affinity MT agent (~1.5 nM) that demonstrated suppression of tumor growth in a variety of cancer animal models. It has been proven safe to use in human subjects and ideal pharmacokinetics and has undergone multiple clinical trials for treatment of glioblastoma and other advanced cancers [22,23]. MPC-6827 crosses the blood–brain barrier in mice, rats and dogs and is distributed rapidly in brain with approximately 14–30 times brain to plasma ratios [24]. O-desmethyl-MPC was the major metabolite of MPC-6827 in humans [23]. Therefore, PET radiolabeling of MPC-6827 at this site probably lead to non-radioactive metabolites and may not interfere with the binding outcome [23,25]. Although clinical outcome suggests that the drug as single agent or combination may have limited success in cancer therapy [26], high brain penetration, lack of multiple drug resistance and established safety profile in humans are the merits of [¹¹C]MPC-6827 as a potential CNS PET imaging agent.

To study MT destabilization and its progression in all dementia disorders including AD, we developed the first brain-penetrating PET radiopharmaceutical, [¹¹C]MPC-6827 [27], and evaluated its imaging efficacy in rodents and nonhuman primate models of AD [27–30]. Additionally, our new *in vitro*, *in vivo* and *ex vivo* mechanistic studies showed that [¹¹C]MPC-6827 uptake is higher to destabilized MTs than stabilized MTs and that the uptake increases with brain A β /tau burden [31]. Postmortem studies on patients with confirmed AD showed higher radiopharmaceutical uptake than the cognitively normal age-matched controls [31]. Given the extensive work published from our group on [¹¹C]MPC-6827, the next steps would be to quantify its binding and metabolic characteristics in target (brain) and plasma—these data will strengthen its potential as a CNS PET radiopharmaceutical. Additionally, to further translate the radiopharmaceutical's promise to clinical settings, we must first characterize its binding and pharmacokinetic properties, including binding constants, plasma and brain metabolism, and stability. Here, we report *in vitro*, *in vivo* and *ex vivo* findings on [¹¹C]MPC-6827 binding and metabolism in rodents.

2. Materials and Methods

2.1. Radiochemistry

[¹¹C]MPC-6827 was produced based on our previously published methods with slight modifications to better shorten reaction times [27]. Briefly, Wake Forest PET Center GE-PETtrace-800 cyclotron generated [¹¹C]CO₂ was converted to [¹¹C]methane through nickel catalyst at 360 °C with GE-FXC radiochemistry module. [¹¹C]methyl iodide (MeI) was formed from the reaction of [¹¹C]methane with gaseous iodine (I₂) at 760 °C. The desmethyl precursor (0.8–1 mg) and 5 μ L 5 N NaOH solution were heated for 3 min at 80 °C in a closed reaction glass vial, post [¹¹C]MeI delivery. Then, 0.7 mL of HPLC mobile phase was used to quench the reaction mixture, which was then transferred onto a C18 Phenomenex ODS (250 \times 10 mm, 10 μ) semi-preparative HPLC column for purification of [¹¹C]MPC-6827. HPLC mobile phase solution consisted of acetonitrile and 0.1 M aqueous ammonium formate solution (4:6), pH 6.0–6.5, UV λ_{\max} of 254 nm, and a 5.0 mL/min flow rate. The final radiopharmaceutical, [¹¹C]MPC-6827 with a retention time (Rt) of 8–9 min, was collected in a round bottom flask preloaded with sterile water (~50 mL), and then allowed to pass through a C18 SepPak cartridge (WAT036800, Waters) to retain the desired product. [¹¹C]MPC-6827 was eluted from the radioactive cartridge with ethanol (1.0 mL) and aqueous saline solution to a final concentration of 10% ethanol in saline. The product was directly collected into a clean sterile final product vial (FPV) through a 0.22 μ m Millipore sterile filter (R1AB86553, Millipore Corp.) for QC analyses and further biological studies. The pH of [¹¹C]MPC-6827 was determined using pH paper, and the final purity was determined using an analytical quality control (QC) HPLC system (C18 Phenomenex HPLC column [250 \times 4.6 mm, 5 μ]) and UV λ_{\max} of 254 nm and a flow rate of 1 mL/min. The QC mobile phase consisted of acetonitrile and 0.1 M aqueous ammonium formate solution (6:4) with a pH 6.0–6.5. [¹¹C]MPC-6827 was validated by performing a routine

co-injection with the non-radioactive standard MPC-6827. Quality assessments including specific activity, radiochemical purities and associated mass were determined at end of synthesis of the final product, [^{11}C]MPC-6827 absorption and standard calibration peak curves (UV $\lambda_{\text{max}} = 254 \text{ nm}$).

2.2. Lipophilicity (LogP)

The sample (2 mL) containing 3.7 MBq [^{11}C]MPC-6827 in PBS buffer, pH 7.4 was mixed with 2 mL 1-octanol, vortexed for 10 min, followed by centrifugation at $5000 \times g$ for 5 min. The top layer (organic) and the bottom (aqueous) layers were separated and transferred into different tubes. All the tubes, including the control tube, were γ -counted and % of radiopharmaceutical in each solvent was determined to calculate LogP.

2.3. Serum Stability

[^{11}C]MPC-6827 (~ 37 – 40 MBq) was added to human serum to bring the final volume to 1 mL *ex vivo* followed by incubation at $37 \text{ }^\circ\text{C}$. [^{11}C]MPC-6827 and the radioactive serum mixture ($\sim 50 \text{ }\mu\text{L}$) were injected into a QC-HPLC (analytical reverse phase Phenomenex HPLC column, $250 \times 4.6 \text{ mm}$; $5 \text{ }\mu$ and UVmax = 254 nm ; flow rate = 1.0 mL/min ; mobile phase = 60% acetonitrile and 40% 0.1 M aqueous ammonium formate [pH 6.0–6.5] solution; Rt = 5–6 min) at 5 min, 30 min, 1 h, 1.5 h, 2 h, and 3 h after radiopharmaceutical synthesis.

2.4. Binding Constants

For *in vitro* autoradiography experiments, mouse brain tissues were sectioned sagittally using a Leica cryostat at $20 \text{ }\mu\text{m}$ thickness, mounted onto SuperfrostTM Plus slides. Sections were stored at $-80 \text{ }^\circ\text{C}$ until further use. Before incubation for 30 min at room temperature with [^{11}C]MPC-6827, sections were kept for thawing for 10 min followed by rehydration in PBS, pH 7.4 for 5 min. Different concentrations of [^{11}C]MPC-6827 were used (63.5, 31.75, 15.87, 7.9, 3.95, 1.97, 0.98, and 0.49 nM) in PBS for the experiment. Adjacent sections were incubated with the same concentration range of [^{11}C]MPC-6827 containing 200 μM MPC-6827. Brain sections were washed in PBS ($4 \times 3 \text{ min}$) and briefly dipped in water. After drying, the sections were exposed to a BAS IP SR 2025 E imaging plate for 10 h. Typhoon Phosphor imaging system was used to scan the plate. Image analysis and quantification was carried out using Fiji (ImageJ, NIH).

The homologous binding assay was carried out with [^{11}C]MPC-6827 and unlabeled MPC-6827 as a blocking agent. Briefly, brain homogenate was prepared from normal male mice ($n = 6$, age 4–5 months) and stored as homogenate solutions (40 mg/mL). The homogenate solution was diluted in PBS buffer, pH 7.4 to a final concentration of 10 μg protein in 250 μL solution per sample. A 50 μL aliquot from a series of [^{11}C]MPC-6827 solutions at increasing concentrations (2.5, 5, 10, 15, 20, 25, 40 and 60 nM) was added to each sample tube. Next, 50 μL aliquots of MPC-6827 standard solution (200 μM) and appropriate amounts of binding buffer were added to each sample to reach a final volume of 250 μL per sample. All the samples were incubated at $37 \text{ }^\circ\text{C}$ for 30 min, then transferred to a 96-well filter plate (PerkinElmer) and washed with PBS buffer (200 μL). The filters were dried at $55 \text{ }^\circ\text{C}$ for 10 min, harvested and γ -counted using the PerkinElmer γ -counter. Counts-per-minute (CPM) values from the γ counter were decay-corrected and converted to fmol/mg values. Specific binding data were fitted nonlinearly to estimate the K_d and B_{max} (maximum specific binding) values from Graphpad Prism v9.3.1.

2.5. Plasma Metabolite Assays

Having demonstrated its lipophilicity, serum stability and binding constants *in vitro* and *ex vivo*, the next studies focused on the metabolic stability of [^{11}C]MPC-6827 in rat brain and plasma tissues *in vivo*. The percentage of [^{11}C]MPC-6827 radioactivity in rat plasma (male Sprague-Dawley rats, $n = 4$ per time point) was determined by C18 HPLC system. Around 0.5 mL of blood samples was drawn from rats at 5, 15, 30, 60 and 90 min after radiopharmaceutical injection. Plasma (0.2 mL) was separated from blood samples via

centrifugation, and then added to acetonitrile (0.3 mL), vortexed (~10 s) and centrifuged at 14,000 rpm (for 5 min). The resulting supernatant liquid (0.3 mL) was separated and diluted with water (0.3 mL), and the radioactivity was measured via a γ -counter before being injected into the same QC HPLC column conditions, equipped with a radioactivity detector. Radioactive metabolite and parent radiopharmaceutical samples were collected, gamma counted and corrected for background radioactivity to measure parent concentration/percentage in the plasma at various time points. A QC sample of [^{11}C]MPC-6827 was injected at the beginning and end of the study to ensure that the parent retention time had not shifted during metabolite analysis. The metabolite fractions per time point were calculated by dividing the fractions corresponding to radioactivity counts of the parent radiopharmaceutical with total HPLC fraction counts.

2.6. Brain Metabolite Assays

The whole brain was harvested from male Sprague–Dawley rats ($n = 4$ per time point) to determine metabolite analysis. Excess blood was blotted; brain removed and carefully homogenized on ice, and radioactivity extracted by adding acetonitrile (1.2 mL) and homogenized again. An aliquot of this brain homogenate (1.0 mL) was centrifuged to pellet the debris. The clear supernatant (0.2 mL) was diluted with distilled water (0.2 mL) for HPLC injection as described above at the same time points: 5, 15, 30, 60 and 90 min after radiopharmaceutical administration.

3. Results

High-quality [^{11}C]MPC-6827 was produced [27], with a radiochemical yield of ~45% in >99% radiochemical purity and specific activity of >350 GBq/ μmol , decay-corrected to the end of synthesis ($n = 30$). Test–retest property of [^{11}C]MPC-6827 radiochemistry on all the specifications showed statistically significant correlation with $r = 0.67$ ($n = 30$ production runs). The final pH of [^{11}C]MPC-6827 was 6.5–7.0. QC-HPLC analysis showed an average mass per batch production of 10–15 μg , and radiochemical purity was authenticated by co-injection with a nonradioactive MPC-6827, which demonstrated retention time similar to that of [^{11}C]MPC-6827 (Figure 1).

A compound lipophilicity is usually indicated by LogP value [32]. The average percent recovery was ~98%. With a low molecular weight (315.8 g/mol), LogP of [^{11}C]MPC-6827, i.e., octanol/water partition coefficient was $\sim 2.9 \pm 0.02$ ($n = 4$). [^{11}C]MPC-6827 efficiently crosses the blood–brain barrier, as previously reported in our PET imaging study [28].

Serum stability is important for a diagnostic imaging agent as it dictates the metabolic fate of the radiopharmaceutical in plasma and target tissue binding. The *ex vivo* serum stability in a human serum sample at different time-points was analyzed by QC HPLC analysis of aliquots extracted at different time points. At 3.0 h, >95% of the parent radioactive tracer remained intact, which indicates that [^{11}C]MPC-6827 has high serum stability and is suitable for *in vivo* use. (Table 1), with a statistical significance of * $p = 0.05$.

Table 1. Stability of [^{11}C]MPC-6827 in human serum sample *ex vivo*.

Time Point	Radiochemical Purity
15 min	99.5%
30 min	99.3%
60 min	99.0%
90 min	99.0%
120 min	98.4%
180 min	97.6%

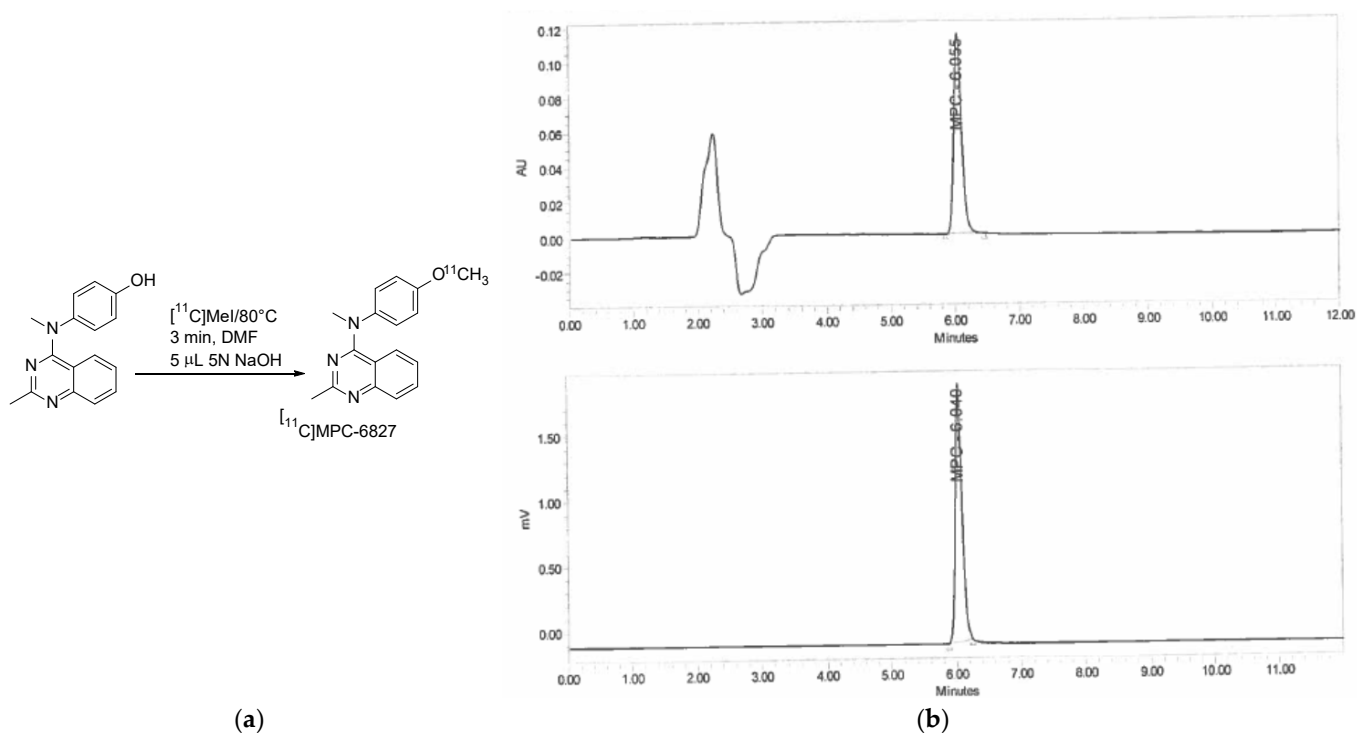


Figure 1. (a) Radiochemical scheme of $[^{11}\text{C}]\text{MPC-6827}$ production; (b) associated QC-HPLC of a co-injection with MPC-6827, QC conditions: Isocratic HPLC with 40% acetonitrile and 60% 0.1 M aqueous ammonium formate solution (pH 6.0–6.5) at a UV wavelength of 254 nm and a flow rate of 1.0 mL/min [reverse-phase Prodigy ODS-3 (250 × 4.6 mm, 5 μm)].

Mouse brain sections were used for performing saturation-binding assay. Co-incubation with non-radioactive MPC-6827 (200 μM) reduced the total binding signal significantly (>70%). A linear increase in nonspecific binding was observed with tracer concentration. Saturation of total binding was observed at radiopharmaceutical concentrations above 20 nM. The K_d value for $[^{11}\text{C}]\text{MPC-6827}$ is determined as 10.03 nM through autoradiography studies. (Figure 2)

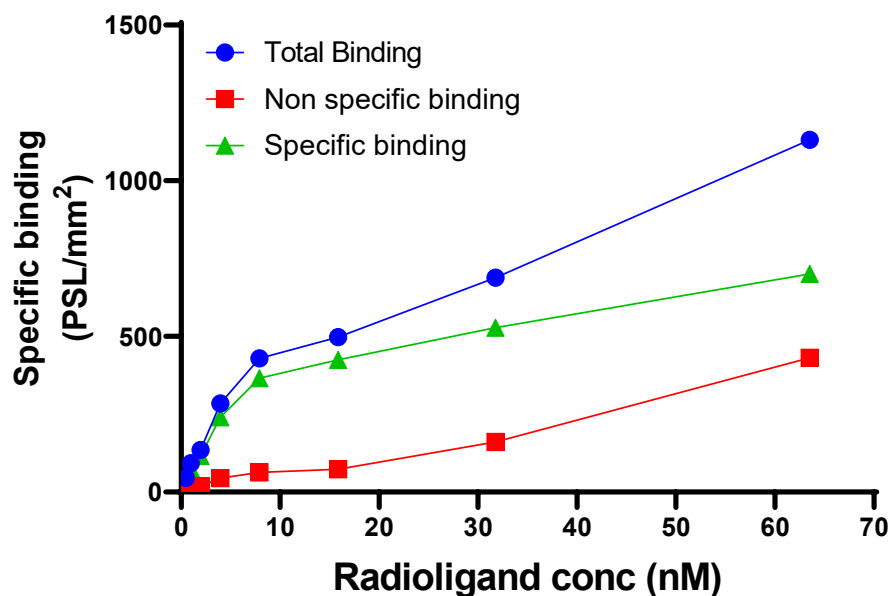


Figure 2. Binding assay of $[^{11}\text{C}]\text{MPC-6827}$ using autoradiography studies.

To determine specific [^{11}C]MPC-6827 binding to mouse brain, a competitive binding assay was performed. The dissociation constant K_d was determined as 15.59 nM with B_{max} of 11.86 (fmol/mg), with a statistical significance of * $p = 0.04$ (Figure 3).

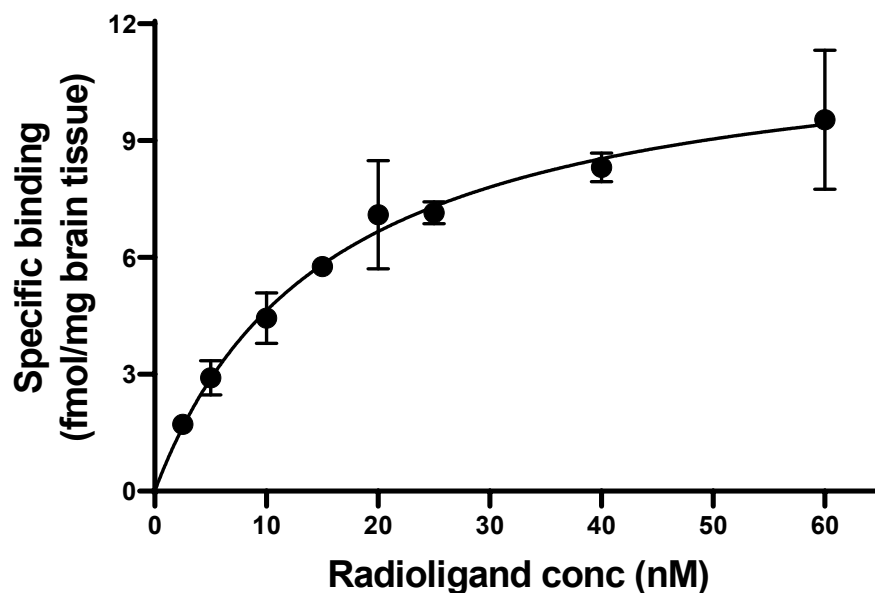


Figure 3. Binding assay of [^{11}C]MPC-6827 in mouse brain homogenates ($n = 6$).

HPLC metabolite analysis [33] of the plasma and brain samples indicated that the percentage of the parent unmetabolized [^{11}C]MPC-6827 was $98.5 \pm 1.5\%$ of total plasma radioactivity at 5 min; $97.7 \pm 0.88\%$ at 15 min; $97.1 \pm 1.1\%$ at 30 min; $95.7 \pm 12.9\%$ at 60 min; and $93.6 \pm 2\%$ at 90 min. With brain samples, the percentage of [^{11}C]MPC-6827 was $99 \pm 0.8\%$ at 5 min; $98.2 \pm 1.5\%$ at 15 min; $97.1 \pm 2.2\%$ at 30 min; $95.4 \pm 1.5\%$ at 60 min; and $94.3 \pm 2.0\%$ at 90 min. HPLC analysis showed a minor peak with a retention time of 3–4 min in both plasma and brain samples. The extraction efficiency and column efficiency for all metabolite analyses were $\sim 92 \pm 1\%$ and test–retest characteristics were statistically significant ($r = 0.75$). (Figure 4).

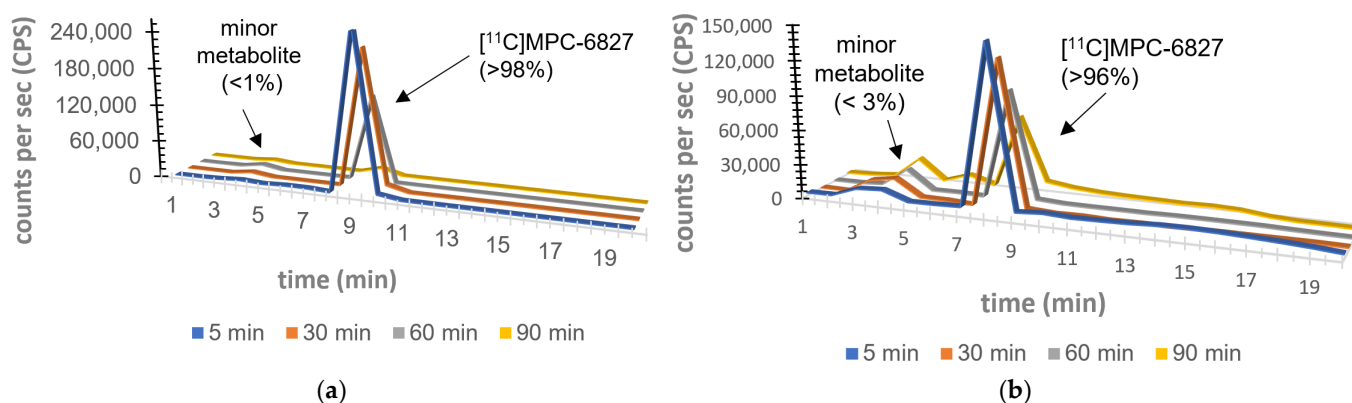


Figure 4. Metabolic assay of [^{11}C]MPC-6827 in rat (a) plasma; (b) brain sample. ($n = 4/\text{time-point}$).

4. Discussion

PET imaging allows us to study biochemical, physiological and pharmacological functions at the cellular and molecular levels [34,35]. Inside the living organism, PET radiopharmaceuticals encounter various chemical effects including redox reactions, hydrolysis, decarboxylation and other conjugation processes. In order to assess PET radiopharmaceutical's imaging efficacy to target regions, it is necessary to quantify the parent

radiopharmaceutical's fraction, binding and kinetics in both plasma and the target (here the brain tissue).

Lipophilicity can be used to estimate how well the CNS-based PET radiopharmaceutical can penetrate the blood–brain barrier [36]. The common way to define lipophilicity is determining LogP, i.e., the partition coefficient of the compound between n-octanol and water. An ideal brain-penetrant radiopharmaceutical has a LogP of 2–3. [^{11}C]MPC-6827 demonstrated a LogP of 2.9, making it possible to cross the blood–brain barrier. To confirm the stability of the radiopharmaceutical *ex vivo*, we applied QC-HPLC method to human serum sample and found that [^{11}C]MPC-6827 was >95% stable in serum for at least 3 h post-injection; highly favorable for a [^{11}C]-based PET isotope with a half-life of 20 min.

Disassociation constant (K_d) and binding specificity (B_{\max}) are two parameters used routinely to measure radiopharmaceutical affinity for the target tissue [37,38]. CNS-based radiopharmaceuticals with K_d and B_{\max} values around 8–16 nM and <500 nM, respectively, showed decent to good target uptake with favorable binding and washing kinetics in neuro PET imaging. [^{11}C]MPC-6827 showed a K_d of 15.59 nM and a B_{\max} of 11.86 (fmol/mg) demonstrating that it is highly suitable for neuroimaging with a favorable pharmacokinetic profile.

As a CNS-based radiopharmaceutical, identification of radiometabolites of [^{11}C]MPC-6827 is vital for translational PET imaging. Metabolic stability in plasma is crucial for the exact quantification of [^{11}C]MPC-6827 that does not hinder the image analyses' approximations for target and reference region in the brain. Determination of parent radiopharmaceutical in plasma at different time points will clarify the trajectory of [^{11}C]MPC-6827 and provide important information on physiological, biochemical and pathological processes. The most widely used technique for the analysis of a radiopharmaceutical is HPLC, combined with radioactivity detectors. Radio-HPLC analyses demonstrated >95% parent radiochemical identity in both brain and plasma samples 90 min post-injection in male Sprague–Dawley rats. At 60 min and 90 min post-injection, radioactivity of plasma displayed a minor peak with a retention time of 3–4 min ([^{11}C]MPC-6827 retention time is 5–6 min) on a C18 HPLC column. The percentage of this peak was $\sim 2.8 \pm 0.04\%$ (at 60 min) and $\sim 3.2\%$ (at 90 min), while the parent radiopharmaceutical remained the major constituent (>97.5%). For the rat brain samples, similar percentages of radiometabolite with a retention time of 3–4 min were seen at 60 min ($\sim 1.6 \pm 0.05\%$) and 90 min ($\sim 2.89 \pm 0.11\%$). As the radiometabolite retention time in both brain and plasma samples was similar, it might be the same metabolite that crosses the blood–brain barrier. While an additional LC-MS analysis is needed to analyze its structure, based on the retention time on a C18 HPLC column, the (minor) metabolite may be slightly more lipophilic than the parent radiopharmaceutical [^{11}C]MPC-6827.

This study demonstrated favorable binding and metabolic parameters of [^{11}C]MPC-6827, following the routine protocols needed to test a CNS-based PET radiopharmaceutical. However, mass spectral analyses are needed to characterize the minor radiometabolite fraction. Next steps would be evaluating the imaging potential of [^{11}C]MPC-6827 in non-human primates and humans using plasma metabolite assays, dosimetry and whole-body distribution.

5. Conclusions

In summary, [^{11}C]MPC-6827, a high-affinity highly selective radiopharmaceutical for imaging MTs, was evaluated to determine its binding, pharmacokinetic stability and metabolic parameters. It exhibited ideal binding characteristics (typical of a CNS radiopharmaceutical) including LogP (2.9), K_d (15.59 nM), and B_{\max} (11.86 fmol/mg). Most importantly, [^{11}C]MPC-6827 showed high serum and metabolic stability (>95%) in rat plasma and brain samples. Metabolic analysis in these samples demonstrated only one minor radiometabolite, at $< \sim 3\%$ with parent radiopharmaceutical >95%. Next steps include radiometabolite analysis and dosimetry studies in non-human primates. [^{11}C]MPC-6827's *in vitro*, *in vivo* and *ex vivo* binding characteristics demonstrate its high potential as a

PET radiopharmaceutical for imaging MTs in humans, aiding in imaging applications for Alzheimer's disease and related dementia and other therapeutic intervention strategies.

Author Contributions: Conceptualization K.K.S.S., A.H.B., B.B., K.K.G., N.D., I.K. and M.M. performed all the experiments including radiochemistry, metabolite analysis, serum stability, saturation-binding, and image analysis under the supervision of K.K.S.S. Data analyses and interpretation was performed by K.K.S.S., A.M. and S.C. The manuscript was compiled and contributed by K.K.S.S., A.H.B. and B.B. All authors have read and agreed to the published version of the manuscript.

Funding: The authors are thankful for funding support for these studies provided by NIH-NIA: R01AG065839 (K.K.S.S.).

Institutional Review Board Statement: All animal experiments were conducted under IACUC-approved protocols in compliance with the guidelines for the care and use of research animals established by Wake Forest Medical School Animal Studies Committee. All the studies were carried out in accordance with approved guidelines for the care and use of research animals established by Wake Forest Medical School Animal Studies Committee.

Informed Consent Statement: No human data.

Data Availability Statement: All the collected data for this manuscript was reported within the article.

Acknowledgments: The authors acknowledge the Translational Imaging Program for their assistance with imaging and equipment support.

Conflicts of Interest: The authors declare no conflict of interest.

References

1. De Ture, M.A.; Dickson, D.W. The neuropathological diagnosis of Alzheimer's disease. *Mol. Neurodegener.* **2019**, *14*, 32. [[CrossRef](#)] [[PubMed](#)]
2. Bloom, G.S. Amyloid- β and Tau: The Trigger and Bullet in Alzheimer Disease Pathogenesis. *JAMA Neurol.* **2014**, *71*, 505–508. [[CrossRef](#)] [[PubMed](#)]
3. Medeiros, R.; Baglietto-Vargas, D.; LaFerla, F.M. The Role of Tau in Alzheimer's Disease and Related Disorders. *CNS Neurosci. Ther.* **2011**, *17*, 514–524. [[CrossRef](#)] [[PubMed](#)]
4. Hooper, C.; Killick, R.; Lovestone, S. The GSK3 hypothesis of Alzheimer's disease. *J. Neurochem.* **2008**, *104*, 1433–1439. [[CrossRef](#)] [[PubMed](#)]
5. Iqbal, K.; Grundke-Iqbal, I. Pharmacological Approaches of Neurofibrillary Degeneration. *Curr. Alzheimer Res.* **2005**, *2*, 335–341. [[CrossRef](#)]
6. Iqbal, K.; Liu, F.; Gong, C.X.; Adel, C.A.; Grundke-Iqbal, I. Mechanisms of tau-induced neurodegeneration. *Acta Neuropathol.* **2009**, *118*, 53–69. [[CrossRef](#)]
7. Garcia, M.L.; Cleveland, D.W. Going new places using an old MAP: Tau, microtubules and human neurodegenerative disease. *Curr. Opin. Cell Biol.* **2001**, *13*, 41–48. [[CrossRef](#)]
8. Goedert, M.; Jakes, R. Mutations causing neurodegenerative tauopathies. *Biochim. Biophys. Acta Mol. Basis Dis.* **2005**, *1739*, 240–250. [[CrossRef](#)]
9. Baird, F.J.; Bennett, C.L. Microtubule Defects and Neurodegeneration. *J. Genet. Syndr. Gene Ther.* **2013**, *4*, 203. [[CrossRef](#)]
10. Franker, M.A.; Hoogenraad, C.C. Microtubule-based transport—Basic mechanisms, traffic rules and role in neurological pathogenesis. *J. Cell Sci.* **2013**, *126*, 2319–2329. [[CrossRef](#)]
11. Hinckelmann, M.-V.; Zala, D.; Saudou, F. Releasing the brake: Restoring fast axonal transport in neurodegenerative disorders. *Trends Cell Biol.* **2013**, *23*, 634–643. [[CrossRef](#)] [[PubMed](#)]
12. Beharry, C.; Cohen, L.S.; Di, J.; Ibrahim, K.; Briffa-Mirabella, S.; Adel, C.A. Tau-induced neurodegeneration: Mechanisms and targets. *Neurosci. Bull.* **2014**, *30*, 346–358. [[CrossRef](#)] [[PubMed](#)]
13. Encalada, S.E.; Goldstein, L.S. Biophysical Challenges to Axonal Transport: Motor-Cargo Deficiencies and Neurodegeneration. *Annu. Rev. Biophys.* **2014**, *43*, 141–169. [[CrossRef](#)]
14. Butner, K.A.; Kirschner, M.W. Tau protein binds to microtubules through a flexible array of distributed weak sites. *J. Cell Biol.* **1991**, *115*, 717–730. [[CrossRef](#)]
15. Wang, J.-Z.; Xia, Y.-Y.; Grundke-Iqbal, I.; Iqbal, K. Abnormal Hyperphosphorylation of Tau: Sites, Regulation, and Molecular Mechanism of Neurofibrillary Degeneration. *J. Alzheimer's Dis.* **2013**, *33* (Suppl. 1), S123–S139. [[CrossRef](#)] [[PubMed](#)]
16. Bamburg, J.R.; Bloom, G.S. Cytoskeletal pathologies of Alzheimer disease. *Cell Motil. Cytoskelet.* **2009**, *66*, 635–649. [[CrossRef](#)]
17. Dubey, J.; Ratnakaran, N.; Koushika, S.P. Neurodegeneration and microtubule dynamics: Death by a thousand cuts. *Front. Cell. Neurosci.* **2015**, *9*, 343. [[CrossRef](#)]

18. Brunden, K.R.; Lee, V.M.; Smith, A.B., 3rd; Trojanowski, J.Q.; Ballatore, C. Altered microtubule dynamics in neurodegenerative disease: Therapeutic potential of microtubule-stabilizing drugs. *Neurobiol. Dis.* **2017**, *105*, 328–335. [[CrossRef](#)]
19. Maschio, C.; Ni, R. Amyloid and Tau Positron Emission Tomography Imaging in Alzheimer’s Disease and Other Tauopathies. *Front. Aging Neurosci.* **2022**, *14*, 838034. [[CrossRef](#)]
20. Chételat, G.; Arbizu, J.; Barthel, H.; Garibotto, V.; Law, I.; Morbelli, S.; van de Giessen, E.; Agosta, F.; Barkhof, F.; Brooks, D.J.; et al. Amyloid-PET and 18F-FDG-PET in the diagnostic investigation of Alzheimer’s disease and other dementias. *Lancet Neurol.* **2020**, *19*, 951–962. [[CrossRef](#)]
21. Rajmohan, R.; Reddy, P.H. Amyloid-Beta and Phosphorylated Tau Accumulations Cause Abnormalities at Synapses of Alzheimer’s disease Neurons. *J. Alzheimer’s Dis.* **2017**, *57*, 975–999. [[CrossRef](#)] [[PubMed](#)]
22. Kasibhatla, S.; Baichwal, V.; Cai, S.X.; Roth, B.; Skvortsova, I.; Skvortsov, S.; Lukas, P.; English, N.M.; Sirisoma, N.; Drewe, J.; et al. MPC-6827: A Small-Molecule Inhibitor of Microtubule Formation That Is Not a Substrate for Multidrug Resistance Pumps. *Cancer Res* **2007**, *67*, 5865–5871. [[CrossRef](#)]
23. Grossmann, K.F.; Colman, H.; Akerley, W.A.; Glantz, M.; Matsuoko, Y.; Beelen, A.P.; Yu, M.; De Groot, J.F.; Aiken, R.D.; Olsen, J.J.; et al. Phase I trial of verubulin (MPC-6827) plus carboplatin in patients with relapsed glioblastoma multiforme. *J. Neuro-Oncol.* **2012**, *110*, 257–264. [[CrossRef](#)]
24. Mauck, K.; Demie, L.; Roman, O.; Fotheringham, L.; Middleton, S.; Mather, G. MPC-6827, a small molecule inhibitor of microtubule formation: Pharmacokinetics in Nu/+ mice, Sprague Dawley rats and beagle dogs following intravenous administration. *Cancer Res.* **2005**, *65*, 806.
25. Chamberlain, M.C.; Grimm, S.; Phuphanich, S.; Recht, L.; Zhu, J.Z.; Kim, L.; Rosenfeld, S.; Fadul, C.E.; Brain Tumor Investigational Consortium. A phase 2 trial of verubulin for recurrent glioblastoma: A prospective study by the brain tumor investigational consortium (BTIC). *J. Neuro-Oncology* **2014**, *118*, 335–343. [[CrossRef](#)]
26. Pérez-Pérez, M.-J.; Priego, E.-M.; Bueno, O.; Martins, M.S.; Canela, M.-D.; Liekens, S. Blocking Blood Flow to Solid Tumors by Destabilizing Tubulin: An Approach to Targeting Tumor Growth. *J. Med. Chem.* **2016**, *59*, 8685–8711. [[CrossRef](#)] [[PubMed](#)]
27. Kumar, J.S.D.; Sai, K.K.S.; Prabhakaran, J.; Oufkir, H.R.; Ramanathan, G.; Whitlow, C.T.; Dileep, H.; Mintz, A.; Mann, J.J. Radiosynthesis and in Vivo Evaluation of [¹¹C]MPC-6827, the First Brain Penetrant Microtubule PET Ligand. *J. Med. Chem.* **2018**, *61*, 2118–2123. [[CrossRef](#)]
28. Damuka, N.; Czoty, P.W.; Davis, A.T.; Nader, M.A.; Nader, S.H.; Craft, S.; Macauley, S.L.; Galbo, L.K.; Epperly, P.M.; Whitlow, C.T.; et al. PET Imaging of [¹¹C]MPC-6827, a Microtubule-Based Radiotracer in Non-Human Primate Brains. *Molecules* **2020**, *25*, 2289. [[CrossRef](#)] [[PubMed](#)]
29. Damuka, N.; Orr, M.; Czoty, P.W.; Weiner, J.L.; Martin, T.J.; Nader, M.A.; Bansode, A.H.; Pathirannahel, B.S.L.; Mintz, A.; Macauley, S.L.; et al. Effect of ethanol and cocaine on [¹¹C]MPC-6827 uptake in SH-SY5Y cells. *Mol. Biol. Rep.* **2021**, *48*, 3871–3876. [[CrossRef](#)]
30. Damuka, N.; Martin, T.J.; Bansode, A.H.; Krizan, I.; Martin, C.W.; Miller, M.; Whitlow, C.T.; Nader, M.A.; Sai, K.K.S. Initial Evaluations of the Microtubule-Based PET Radiotracer, [¹¹C]MPC-6827 in a Rodent Model of Cocaine Abuse. *Front. Med.* **2022**, *9*, 817274. [[CrossRef](#)] [[PubMed](#)]
31. Damuka, N.; Orr, M.E.; Bansode, A.H.; Krizan, I.; Miller, M.; Lee, J.; Macauley, S.L.; Whitlow, C.T.; Mintz, A.; Craft, S.; et al. Preliminary mechanistic insights of a brain-penetrant microtubule imaging PET ligand in a tau-knockout mouse model. *EJNMMI Res.* **2022**, *12*, 41. [[CrossRef](#)] [[PubMed](#)]
32. Wilson, A.A.; Jin, L.; Garcia, A.; Da Silva, J.N.; Houle, S. An admonition when measuring the lipophilicity of radiotracers using counting techniques. *Appl. Radiat. Isot.* **2000**, *54*, 203–208. [[CrossRef](#)] [[PubMed](#)]
33. Padakanti, P.K.; Zhang, X.; Jin, H.; Cui, J.; Wang, R.; Li, J.; Flores, H.P.; Parsons, S.M.; Perlmutter, J.S.; Tu, Z. In Vitro and In Vivo Characterization of Two C-11-Labeled PET Tracers for Vesicular Acetylcholine Transporter. *Mol. Imaging Biol.* **2014**, *16*, 773–780. [[CrossRef](#)]
34. Phelps, M.E.; Hoffman, E.J.; Mullani, N.A.; Ter-Pogossian, M.M. Application of annihilation coincidence detection to transaxial reconstruction tomography. *J. Nucl. Med.* **1975**, *16*, 210–224. [[PubMed](#)]
35. Ter-Pogossian, M.M.; Phelps, M.E.; Hoffman, E.J.; Mullani, N.A. A Positron-Emission Transaxial Tomograph for Nuclear Imaging (PETT). *Radiology* **1975**, *114*, 89–98. [[CrossRef](#)] [[PubMed](#)]
36. Waterhouse, R.N. Determination of lipophilicity and its use as a predictor of blood–brain barrier penetration of molecular imaging agents. *Mol. Imaging Biol.* **2003**, *5*, 376–389. [[CrossRef](#)]
37. Hulme, E.C.; Trevethick, M.A. Ligand binding assays at equilibrium: Validation and interpretation. *Br. J. Pharmacol.* **2010**, *161*, 1219–1237. [[CrossRef](#)]
38. Eckelman, W.C.; Reba, R.C.; Gibson, R.E.; Rzeszotarski, W.J.; Vieras, F.; Mazaitis, J.K.; Francis, B. Receptor-binding radiotracers: A class of potential radiopharmaceuticals. *J. Nucl. Med.* **1979**, *20*, 350–357.

Disclaimer/Publisher’s Note: The statements, opinions and data contained in all publications are solely those of the individual author(s) and contributor(s) and not of MDPI and/or the editor(s). MDPI and/or the editor(s) disclaim responsibility for any injury to people or property resulting from any ideas, methods, instructions or products referred to in the content.